THE JOURNAL OF PHYSICAL CHEMISTRY B

ARTICLE

pubs.acs.org/JPCB

High Internal Phase Emulsions under Shear. Co-Surfactancy and Shear Stability

Peter N. Yaron,[†,§] Andrew J. Scott,[†] Philip A. Reynolds,[†] Jitendra P. Mata,[†,‡] and John W. White*[,†]

[†]Research School of Chemistry, Australian National University, Canberra, ACT 0200, Australia

[‡]Bragg Institute, ANSTO, Locked Bag 2001, Kirrawee DC, NSW 2232, Australia

[§]Department of Chemical Engineering, Carnegie Mellon University, Pittsburgh, Pennsylvania 15213, United States

S Supporting Information

ABSTRACT: Large changes in the rheology of high-internal phase aqueous-in-oil emulsions (HIPEs) using an oil-soluble polyisobutylene-based primary surfactant (PIBSA) are provoked by very small quantities of water-soluble polyamide-based cosurfactants (PAM with C_{12}, C_{14}, and C_{16} tails). The structural origin of this was studied using small-angle neutron scattering (SANS) from sheared emulsions, with simultaneous in situ rheology measurements. The PAM drastically lowers the droplet−oil interfacial tension by displacing PIBSA, causing large droplet deformation under shear and much lowered emulsion yield stress. With PAM, the surfactant monolayer at the droplet surface becomes more responsive to droplet shape change and redistributes in response to shear which the PIBSA-only system does not. Although it is oil-insoluble, PAM also reaches the nanoscale PIBSA micelles in the oil phase, changing micelle size and content in ways predictable from the hydrophilicity of the different PAMs. PAM does not, however, strongly affect the viscosities at high shear rates; shear thinning and thickening are unaffected. Droplet size, droplet−droplet flattening, and linkage determine the viscosities observed, more so than droplet−oil interfacial tension. We infer from this that the droplet motion under shear does not involve much transient droplet deformation as the droplets move by each other.

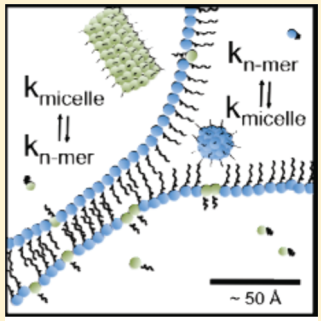

Droplet distortion

INTRODUCTION

We report the change in rheological behavior of high-internal phase emulsions (HIPEs) under shear when a water-soluble polyacrylamide cosurfactant is added by tracking the locations of the surfactant and cosurfactant together as a function of shear using small-angle neutron scattering (SANS) and in situ rheological measurements. Similar experiments on the oil-soluble surfactant-only emulsion have shown the microscopic origin of the macroscopically observed shear thinning and thickening.[1] Cosurfactants are of importance in many commercial applications because they allow the physical and chemical properties of an emulsion to be varied without sacrificing function. This work follows a series of papers analyzing the structural variation and stability of emulsions using polyisobutylene-based (PIBSA) surfactants alone, under static and shear conditions. Their sensitivity to aqueous/oil phase ratios, surfactant concentration, surfactant molecular weight, and polydispersity has been defined.[1−8] The emulsions consist of almost spherical micron-scale, highly polydisperse, aqueous droplets dispersed in a continuous oil phase with aqueous/oil phase ratios of about 9:1.

The stability and rheology of single surfactant (PIBSA) stabilized emulsions is closely linked to the surfactant's distribution around an individual droplet, droplet deformation, and migration between the various surfactant reservoirs in the emulsion upon the application of shear stress.[1] Even at the low-surfactant limit of emulsion formation and stability, a large percentage of surfactant lies in the continuous oil phase dissolved as small n-mers or as larger reverse micelles which play an important part in stabilizing of the emulsion under shear.[1−6] Steady shear on these emulsions reduces the number of reverse micelles present in the continuous oil phase to provide the surfactant needed to cover the newly formed surface area as the emulsion refines to smaller droplet sizes. This is accomplished by two processes. The first draws soluble surfactant from the oil phase to the interface and lowers the concentration of dissolved n-meric surfactant.[1] In parallel, oil-soluble reverse micelles begin to break up, allowing a shear rate dependent steady state to establish between the surfactant reservoirs and aqueous droplets. The application of low-shear rate recovery intervals allowed the recovery dynamics of the surfactant distribution to be observed. The results showed little reduction of the emulsion interfacial area upon return to its quiescent state, but a large recovery of the reverse micelle volume fraction that indicates that the continuous phase acts as the reservoir of surfactant when the emulsion is under shear.

In the following experiments the cosurfactants produce a new and definable pathology allowing further insight into these systems. We observe and quantify the effect of altering the chain

Received: January 19, 2011
Revised: March 20, 2011
Published: April 18, 2011

ACS Publications © 2011 American Chemical Society

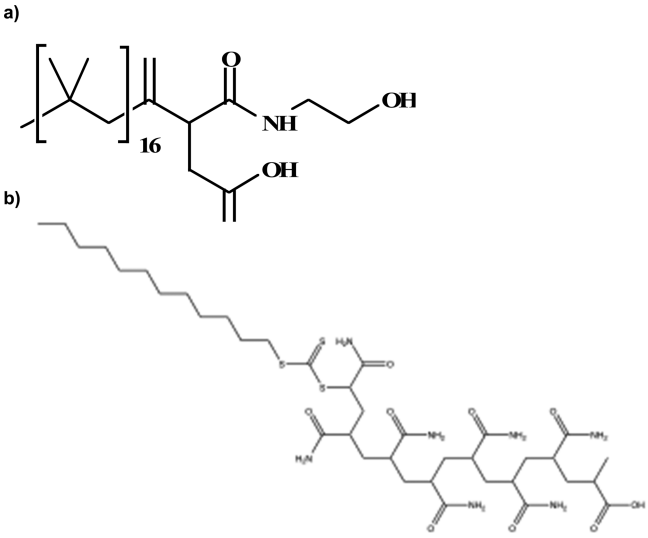

Figure 1. (a) A typical PIBSA surfactant molecule. (b) A typical C_{12}-PAM molecule (17-amino-4,6,8,10,12,14-hexacarbamoyl-16-(dodecylthiocarbonothioylthio)-2-methyl-17-oxoheptadecanoic acid).

length and concentration of water-soluble polyacrylamide based cosurfactants (C_{12}-PAM, C_{14}-PAM, and C_{16}-PAM) on the properties of the high internal phase PIBSA emulsions under shear.

EXPERIMENTAL SECTION

Materials. The materials used to make the PIBSA-only HIPEs have been described in previous papers.[1−6] (The PIBSA was supplied as a 45% solution in 55% oil.) The three PAM cosurfactants were synthesized by reversible addition−fragmentation chain transfer (RAFT) copolymerization[9] of acrylamide with the RAFT reagents. The ^{1}H and polystyrene calibrated gas-phase chromatography (GPC) M_N values were 848 and 853 with a GPC M_W = 752. Mass spectrometry shows a distribution of molecular weights with from 7 to 11 acrylamide monomer units.[10] Using the peak heights, 80% of the product has a molecular weight between five and seven units. The three RAFT reagents begin with, respectively, $C_{12}H_{25}$-, $C_{14}H_{29}$-, and $C_{16}H_{33}$-normal alkane chains. The final PAM surfactants will be labeled C_{12}-PAM, C_{14}-PAM, and C_{16}-PAM. Typical PIBSA and C_{12}-PAM molecules are shown in Figure 1a and b.

The tacticity of the samples of PAM used are, as yet, undetermined. They are most likely to be atactic compounds formed under the experimental conditions used. The magnitudes of the dipole moments in the axial direction are noteworthy.[10]

The HIPEs used in our experiments were prepared by fast shearing at 80 °C the chosen hexadecane−surfactant mixture, in which the required amount of PAM is suspended, while slowly dropping in the almost-saturated ammonium nitrate solution over 3 min, followed by one minute of further shearing for 90 s. A total of 38 emulsions were prepared in 15 mL quantity, all with a dispersed aqueous phase comprising 90% of the emulsion volume. A total of 18 emulsions contained 0.3% (by volume) of PIBSA, and 20 contained 1% of PIBSA. The volume percentages of the PAM varied from 0.005% to 0.5%. Table 1 of the Supporting Information lists the individual contents, together with those for the four PIBSA-only emulsions from the previous experiment.[1]

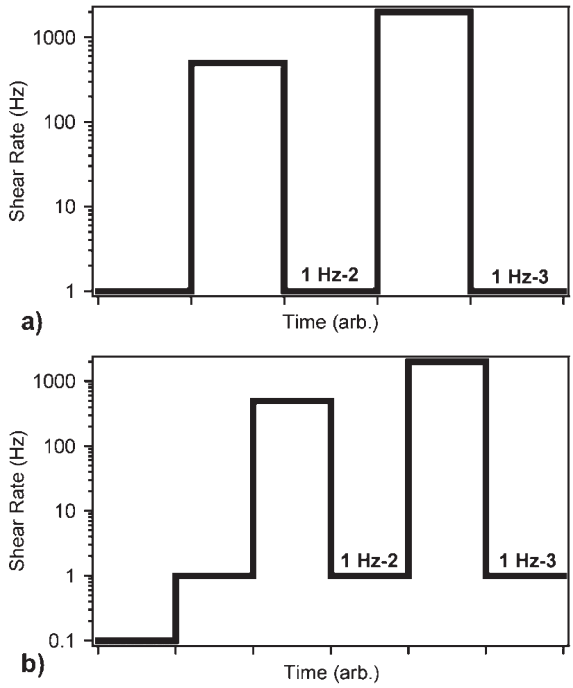

Figure 2. Shear profile used for the (a) PIBSA/C_{12}-PAM emulsions and (b) PIBSA/C_{14}, C_{16}-PAM emulsions. Data collection times of the individual emulsions vary slightly because of changes in the neutron beam flux which affect the total time needed to collect the necessary integrated neutron count deemed necessary for an acceptable signal-to-noise ratio in the SANS signal.

To test PAM solubility in the oil phase, the three different chain length PAMs were dissolved, at 1% concentration by volume, in ammonium nitrate solution, in which they were readily soluble. Hexadecane was added to make a two-phase sample with an aqueous/oil volume ratio of 9:1. After gentle shaking (to avoid any possible emulsification) the three samples were left for four days. In all samples the aqueous phase remained a bright yellow, while the hexadecane phase was completely colorless as verified by UV−vis spectroscopy. This result indicates that the PAM chain length does not alter its insolubility in hexadecane. Small-angle X-ray scattering at ESRF (Grenoble) shows the presence of cylindrical micelles in saturated ammonium nitrate/water solutions.[11] This suggests that PAM surfactant resides in the aqueous phase as small n-mers and micelles.

Rheology. The HIPEs used in our experiments were designed to maintain the same relative internal-phase volume fraction while changing the concentrations of surfactant and cosurfactant. A minimum of 24 h after manufacturing was allowed to let the emulsion to recover any microstructure. Sample handling followed a procedure described previously to minimize shearing to the emulsion.[1] Rheology experiments were conducted in situ on the LOQ beamline (Rutherford Appleton Laboratory, ISIS Facility, Chilton, UK)[12] using an Anton-Paar Physica MCR501 Rheometer. It uses a Couette cell geometry, which is comprised of two concentric quartz cylinders, with an inner stator (radius 25 mm) and an outer rotor, with a 0.5 mm gap between cylinders and a bottom gap of 0.56 μm. We followed an experimental procedure described previously.[1] The shear profiles used in the experiments, illustrated as a function of shear rate, D, and time in Figure 2, were modified slightly from previous experiments.[1] To

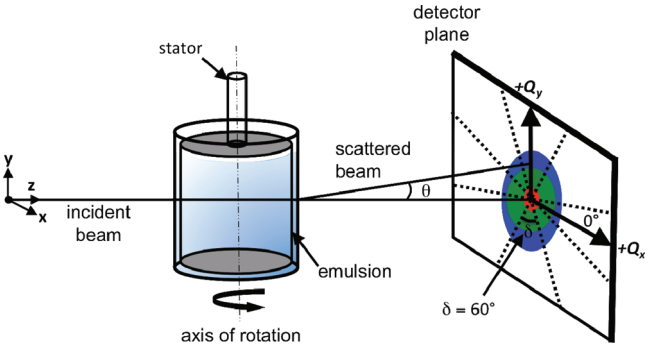

Figure 3. Illustration of the SANS/in situ rheometry experimental setup. The dashed lines and shaded areas on the detector plate indicate the partition of the integrated signal into horizontal (Q_x) and vertical components (Q_y) for calculations of droplet anisotropy.

obtain a better estimate of the viscosity at zero shear, η_0, an initial shear rate of 0.1 Hz was used. The 1 Hz shearing runs were implemented to eliminate any shear history of the emulsion without causing further changes in the distribution of the surfactant due to droplet breakup. The number of shearing and recovery intervals was decreased, and the duration increased in some intervals to allow for equilibration of the emulsions under steady shear.

Small-Angle Neutron Scattering Experiments. Measurements were conducted at Rutherford Appleton Laboratory ISIS facility LOQ beamline using incident neutron wavelengths between 2.2 and 10 Å, sorted by time-of-flight, with a sample detector distance of 4.1 m. This gives a Q-range between 0.009 and 0.24 $Å^{-1}$. The 1 mm sample total path length (front and back of Couette cell), and the low-scattering nature of the samples, ensured transmissions greater than 90%, and thus no need for multiple scattering corrections. Emulsions were produced in a contrast-matched (CM) and contrast unmatched (UM) varieties at each surfactant concentration to highlight the distribution of surfactant in the oil-phase and at the droplet interface. CM samples were produced by matching the high scattering length densities (SLD) of the aqueous phase ammonium nitrate/deuterium oxide (AN/D_2O) with that of the oil phase (hexadecane/*d*-hexadecane) so that both then contrast strongly with the scattering from the low SLD surfactants -0.06×10^{-6} $Å^{-2}$ and 0.092×10^{-6} $Å^{-2}$ for PIBSA and PAM, respectively. UM samples were designed to highlight the aqueous/droplet interface. This was done using hexadecane (-0.43×10^{-6} $Å^{-2}$), contrasting with the high SLD of the AN/D_2O 4.88×10^{-6} $Å^{-2}$. The emulsion constituents are shown in Table 1 (Supporting Information). Neutron data were processed in standard ways described previously,[12,13] to which the reader is referred for details of accuracy, reliability and errors. A D_2O sample run was used for cell/coherent background subtraction. The incoherent background was corrected for during the fitting process by use of a scaled H_2O minus D_2O pair of runs. We should note that much of our discussion is of differences in the same sample at different shear rates. These differences are relatively unaffected by errors in data corrections, which will be very similar for the patterns compared. However absolute values obtained from fits of surface areas, for example, will be less reliable.

Anisotropy in the scattering profiles was analyzed by partitioning the raw data collected from the detector array into horizontal and vertical components in a method described previously.[1] Figure 3 illustrates how the detector data was partitioned and radially integrated. The upper and lower slices give the vertical (Q_y) data, and the left and right slices the horizontal (Q_x).

Small-Angle Neutron Scattering Data Analysis. This work presents data from 38 new and 4 previous emulsions, which produced over 250 isotropic shear dependent SANS profiles and 500 anisotropic profiles, all which have been analyzed and fitted multiple times to obtain reproducible parameters. The model used to fit the SANS data has been utilized and explained extensively before.[1−8] In summary, the total scattering intensity is approximated as the sum of four intensity components shown in eq 1, scattering from the aqueous droplet/oil interface, reverse micelles in the oil continuous phase, bilayers formed during droplet deformation, and an incoherent background. Because of the huge size disparity between aqueous droplets and the reverse micelles the interference term between the interface and micelles is negligible.

$$I(Q)_{\text{tot}} = (1 - \text{frac})I(Q)_{\text{Porod}} + I(Q)_{\text{micelle}} + (\text{frac})I(Q)_{\text{bilayer}} + I(Q)_{\text{bk}} \quad (1)$$

The water droplets' smallest mean radii are several thousand Ångstroms. The lowest accessible Q-range of LOQ is insufficient to detect this droplet interface curvature. Thus, planar models fit the interfacial scattering. The UM emulsions show a Q-dependence close to Porod scattering (Q^{-4} dependence) from the SLD step at the droplet interface, and thus give the droplets' specific surface area. There was a slight but significant deviation from a Porod slope in *Q*, accounted for by invoking formation of a planar aqueous/oil/aqueous bilayer (the beginning of droplet "polygonization") for a small fraction of the surface area, where two droplets have touched and mutually flattened. The fraction of droplet surface flattened is defined in the model by the "frac" parameter in the fitting program. At the lowest *Q* values, frac is the fraction of scattering from a slab (Q^{-2} dependence) compared to the slab scattering plus the Porod scattering from the remaining step oil/aqueous interface (Q^{-4} dependence). The CM emulsions show scattering from the thin slab of low SLD at the interface due to adsorbed surfactant (Q^{-2} dependence).

The model was applied to both the CM and UM data using IGOR PRO routines. The instrumental resolution function was used to appropriately convolute the calculated intensity to compare with the experimental data. There are a large number of free parameters in this model. Since these are the first studies of these particular cosurfactant emulsions we have no a priori knowledge of the parameters, and so the values obtained from the single surfactant data were taken as the starting point for emulsions with the lowest cosurfactant content. The method of releasing each constraint from its fixed value sequentially was then used to decide that the values did not change significantly and to establish the correlations to other parameters. A micelle polydispersity, shell, core SLD, and oil SLD was fixed in the CM data. The reverse micelle volume fraction (ϕ_{micelle}) in the oil, micelle SLD and radius, droplet interfacial surfactant loading ("loading"), and incoherent background remained as the free parameters. In the UM fits, the model was constrained by entering the same fixed values of r_{micelle} and ϕ_{micelle} obtained from CM fits, allowing background, Porod droplet interfacial area (A_V), frac, and micelle SLD to vary. The total number of parameters (9, including two backgrounds) fitted to each UM/CM pair of patterns is large. Attempts to further constrain

parameters were unsuccessful. In particular the micellar radius cannot now be fixed, as in reference 1, since it appears to vary significantly. Another attempt to constrain the total amount of surfactants to that added failed, showing only that besides the PIBSA there are significant amounts of PAM at the droplet interface. Unfortunately we cannot fix how much because the amount of PAM in the aqueous phases is not measured here, unlike the amount of PIBSA in the oil phases, which is defined by the CM data. The fits produced were satisfactory. The values for all $\phi_{micelle}$, A_V, loading, frac, and total amount of surfactant for each shearing interval are the indicators and are listed in the Supporting Information section of this article. It is clear that shear affects the isotropic SANS patterns, and the effects are not small.

Details of the intensity contributions from the micellar scattering and bilayer scattering are described elsewhere.[6,14,15] Because of the anisotropy found in both CM and UM the scattering profiles, the model was also applied to the Q_y integrated scattering intensity to determine if large changes in $r_{micelle}$ values occur.

The refined values of oil interface scattering length densities, micellar volume fraction, and SLD can be used to calculate a total mass of surfactant detected by SANS. After augmentation by the proportion of surfactant dissolved in the oil, known from previous inverse micellar solution SANS studies,[1] we can compare the total amount of surfactant found by scattering with that weighed into the emulsion mix. This is a further test of our modeling procedure. At the highest shear (2000 Hz), we saw in about 50% of cases anomalously reduced values in the background and A_V. These are completely correlated with extremely low viscosity values. It is clear emulsion material was lost from the sample's neutron scattering area, and the emulsion no longer spanned the gap between inner and outer Couette cylinders. Any data showing these effects were not used for analysis.

The following data refinement procedure was used to model fit the CM anisotropic data sets. Since scattering is designed to highlight scattering only from the surfactant components, fitting of these data sets gives an approximate amount of distortion of the micelles under shear. First, a fit was performed on the CM isotropic data with $\phi_{micelle}$ and background as free parameters and fixing $r_{micelle}$ and polydispersity to values obtained from initial fits. This fit provides an approximate value for $\phi_{micelle}$, as we do not expect these values to be affected significantly by anisotropy in the scattering intensity. Using the fixed values obtained from the CM isotropic fits a second fit was performed on the same CM isotropic data with the $\phi_{micelle}$ fixed and the $r_{micelle}$ and polydispersity, background, and A_V as free parameters. These parameters give the $r_{micelle}$ and polydispersity of the CM isotropic data, which is a convolution of I_x and I_y and provides a comparison to the anisotropic data. Constraining $\phi_{micelle}$ and polydispersity using values obtained from the isotropic data and freeing $r_{micelle}$, A_V, and background, the Q_x and Q_y anisotropic data sets were then fitted. These values were then compared to each other and to the corresponding isotropic values as a function of shear.

The refining procedure for the UM anisotropic data was designed to measure the difference in the interfacial specific surface area, A_V, as a function of shear. Using the $r_{micelle}$, polydispersity, and $\phi_{micelle}$ from the CM corresponding anisotropic data, the A_V and background values were free parameters. The values of A_V obtained for Q_x and Q_y were then compared to each other and to the corresponding UM isotropic data as a function of shear.

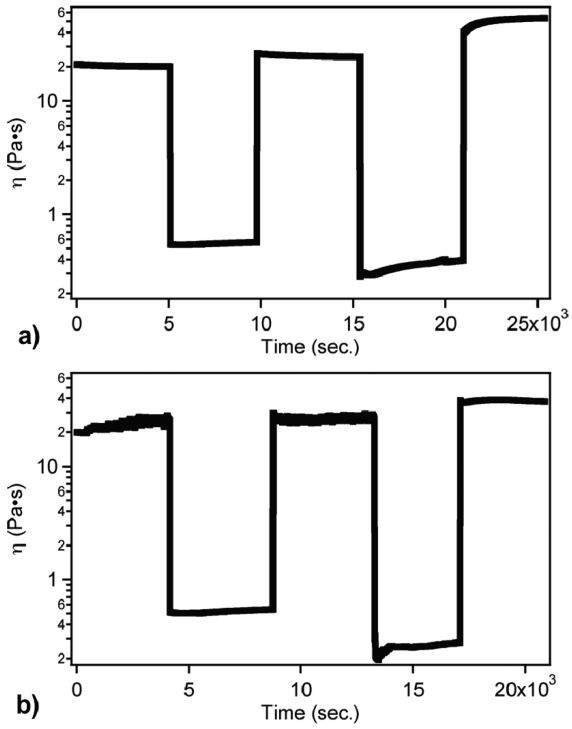

Figure 4. Rheological profiles collected simultaneously during data collection of the SANS data shown in Figure 5 from a 0.3% PIBSA and 0.025% C_{12} PAM neutron contrast matched (CM) (a) and contrast unmatched (UM) (b) emulsion. The differences in elapsed time are due to fluctuations in neutron beam intensity affecting collection times needed to achieve acceptable signal-to-noise ratios for all emulsions.

RESULTS

Rheology. The viscosity versus elapsed time obtained from the applied shear profile is shown in Figure 4 for typical samples. The times of the individual runs vary slightly because of changes in the neutron beam flux which affect the total time needed to accumulate the deemed fixed minimum total integrated neutron count needed for an acceptable signal-to-noise ratio in the SANS signal.

The gross changes in viscosity for each sample can be illustrated by plotting the equilibrium viscosity value at each shear rate versus time. This is extrapolated from the data in each individual run interval using equilibrium viscosity values obtained using a procedure described previously.[1] The rheology results from the cosurfactant emulsions show similar behavior to that of the single surfactant emulsion. So we will only summarize the results here. For a more detailed discussion reference 1 should be consulted. There is a strong shear-thinning regime with increasing shear rate, shear thickening on return to the "resting" 1 Hz shear rate, and (not shown) yield stresses and critical shear rates where droplet dynamics significantly change. Some of the emulsions were allowed to stand for significantly more than 24 h. This aging produced noticeable thickening, detected in the 0.1 Hz shearing runs, but shearing at 1 Hz was sufficient to return all of the emulsions to an equivalent state. Table 2 (Supporting Information) shows the steady state equilibrium shear stress values as a function of emulsion and shear rate applied. The shear stress values are obtained by multiplication of the viscosity values with the applied shear rate. The intersection on the stress axis on a plot of the stress versus

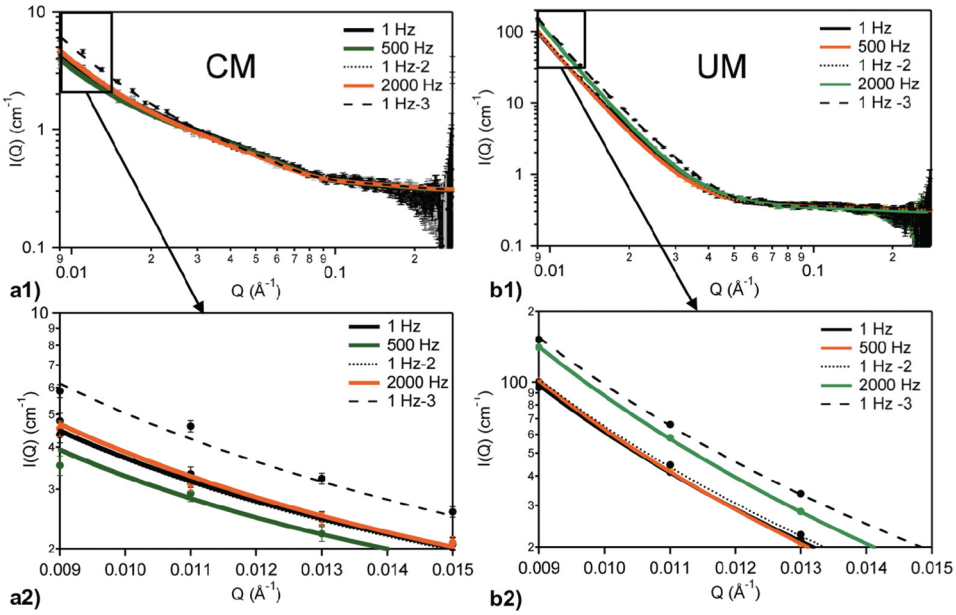

Figure 5. Scattering profiles from a 0.3% PIBSA 0.025% C_{12} PAM neutron contrast matched (CM) (a) and contrast unmatched (UM) (b) emulsion. The inset figures (boxes) enlarged below (a2 and b2) illustrate the change in intensity at low-Q as a function of applied shear. The model free parameter results for these two emulsions are shown in Table 5 of the Supporting Information section. The errors bars associated with the data points in Figure a2 are smaller than the point size.

shear rate of an emulsion can be used to extrapolate a dynamic yield stress, τ_c, which is the value of stress required to induce flow.[16] Extrapolated yield stress values are also listed in the Supporting Information section (Table 3).

Isotropically Averaged Scattering. The data were first treated by making a 360 degree radial average of the scattering patterns to draw broad conclusions on the effect of shear for comparison with the PIBSA-only HIPEs. A typical series of scattering patterns (data points) along with overlaid model fits (solid lines) is shown in Figure 5. The analysis of the SANS data was performed using the model described in the data analysis section and in previous papers.[1−8] We observe in both the CM and UM data that the low-Q intensities increase in value in the 1 Hz recovery interval measurements. As for the PIBSA-only systems, this effect becomes more pronounced as the applied shear is increased above 500 Hz. In the UM scattering data, the intensity at low-Q defines the total interfacial surface area, A_V, of the droplet/oil interface in the emulsion.

The increased intensity of the UM data as a function of applied shear indicates that new surface area was being created, due to the refining of emulsion droplets to smaller sizes. A rough estimate of this from $I(0)$ in the UM data Figure 5b is about a 20% increase in interfacial area. The CM data (Figure 5a) increase in $I(0)$ also shows higher surfactant loading at the interface, as well as the increase in surface area. The surfactant loading in the CM data may be estimated using the UM-derived interfacial surface area combined with the intensity of scattering at low-Q in the corresponding CM emulsion data.

The presence of a flattening in the scattering function ($0.02 < Q/\text{Å}^{-1} < 0.09$ for the CM data is indicative of scattering from the reverse micelles present in the oil phase. In contrast with the PIBSA-only emulsions where micelle size is almost independent of PIBSA concentration, these micelles vary in diameter with concentration of PAM cosurfactant, as well as PAM type. There appears, however, to be little shear dependence of the diameter, but as for the PIBSA-only emulsion, the intensity decreases with increasing shear indicating a decrease in the population of micelles. The location of the emulsion stabilizing surfactant and its redistribution by the shear field can be quantified from the SANS model fits for the CM and UM data. Surfactant loading at the interface and interfacial area increase slowly with shear rate, as for the PIBSA-only emulsions, and the total amount of surfactant found in the emulsion from all of these contributions is also relatively constant.

The values for ϕ_{micelle}, r_{micelle}, and frac for each shearing interval vary similarly to the PIBSA-only emulsions.[8] Model fitted results of the various free parameters, as a function of PAM concentration and interfacial area, are shown in Figures 6−10 and in the Supporting Information section (Tables 4−6). Shear strongly affects the isotropic SANS patterns, and the effects are more pronounced than in the PIBSA-only emulsions.

Anisotropic Scattering as a Function of *Q*. Examination of the two-dimensional scattering profiles shows the presence of asymmetry in the scattering patterns under shear. The intensity of the integrated vertical scattering ($I(Q_y)$) increases relative to the horizontal scattering ($I(Q_x)$), indicative of elongation along the direction of the applied shear. In Figure 9 we have plotted $200(I(Q_y) - I(Q_x))/(I(Q_y) + I(Q_x))$, the percentage relative anisotropy as a function of the applied shear profile, for a typical set of UM data at a shear rate of 500 Hz. The data are also listed in Table 7 (Supporting Information).

We notice that in the UM data there is a increasing degree of anisotropy with increasing shear, which plateaus at 500 Hz, reaching up to 45% and that it is independent of Q. Since our distance resolution in the SANS experiment is much less than the droplet diameter we would expect this Q-independence. In contrast to the PIBSA-only emulsions examined previously, the CM data now also show anisotropy, though smaller than the UM samples. Thus the surfactant distribution is also shear-dependent. The addition of PAM only, qualitatively, introduces anisotropy in the CM data.

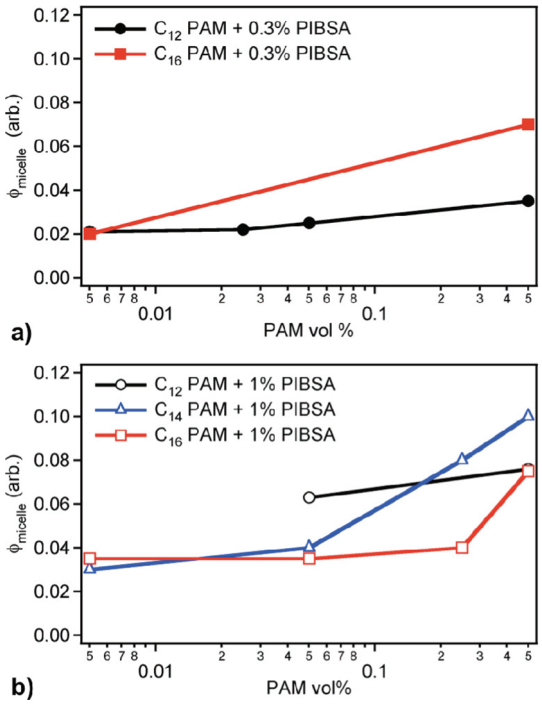

Figure 6. Plot of the micelle volume fraction, $\phi_{micelle}$, at 500 Hz versus the volume fraction of PAM surfactant at a constant PIBSA volume fraction: (a) 0.3% (v/v) PIBSA, (b) 1% (v/v) PIBSA. The errors associated with the ordinate were not included but do not exceed ±0.0009.

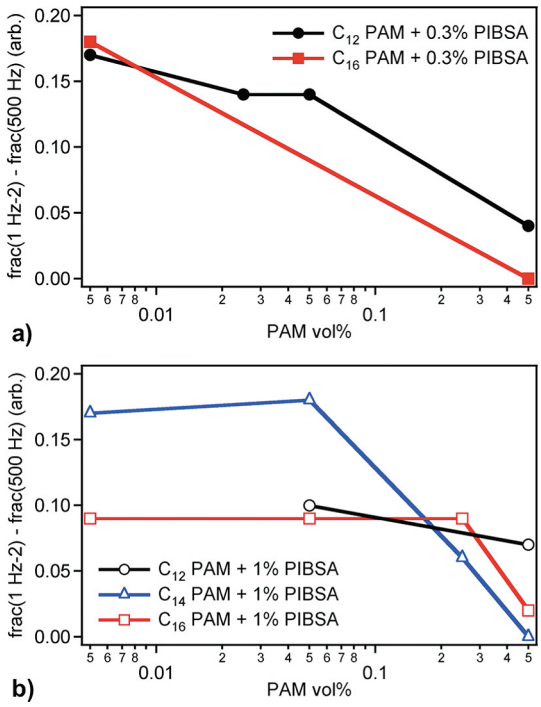

Figure 8. Plots of the change in frac values, Δ frac, (Δ frac = frac(1 Hz) − frac(500 Hz)) from the quiescent state "frac(1 Hz)" and obtained during shear at 500 Hz "frac(500 Hz)" versus PAM surfactant volume fraction at a constant PIBSA volume fraction: (a) 0.3% (v/v) PIBSA, (b) 1% (v/v) PIBSA.

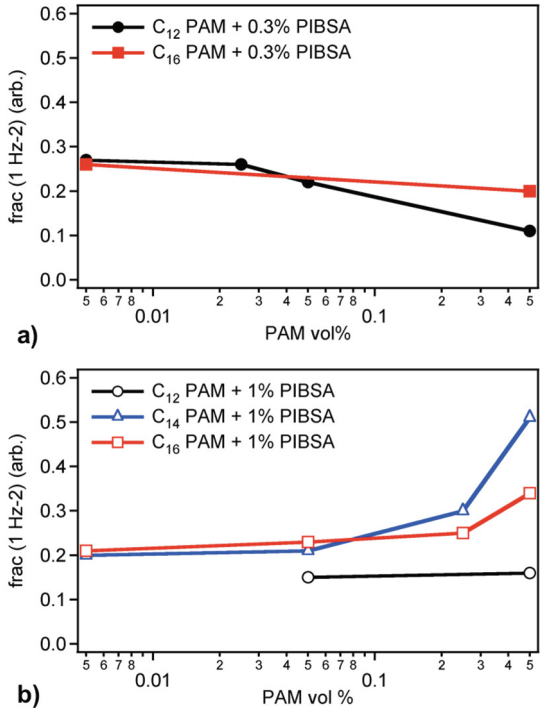

Figure 7. Plots of the frac values obtained during shear at 1 Hz (1 Hz-2) after shear at 500 Hz, versus PAM surfactant volume fraction at a constant PIBSA volume fraction: (a) 0.3% (v/v) PIBSA, (b) 1% (v/v) PIBSA. The errors associated with the ordinate were not included but do not exceed ±0.009.

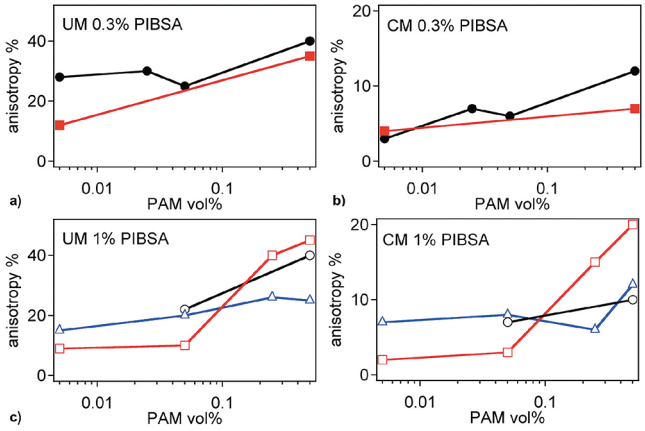

Figure 9. Plot of the anisotropy at 500 Hz versus volume fraction of PAM surfactant for all emulsions. The top figures are the neutron contrast unmatched (a) and contrast matched (b) at a PIBSA volume fraction of 0.3% (v/v). The bottom figures are the neutron contrast unmatched (c) and contrast matched (d) at a constant PIBSA volume fraction of 1% (v/v). The error bars associated with the ordinate have been excluded but do not exceed ±0.00015%. C_{16}-, C_{14}-, and C_{12}-PAM are represented by squares, triangles, and circles respectively, similar to Figures 6−8.

The Q_y and Q_x anisotropy data were fitted separately using our standard model and method described in the previous section to measure any distortion of the micelles from spherical, in addition to the distortion of the much larger aqueous droplets.

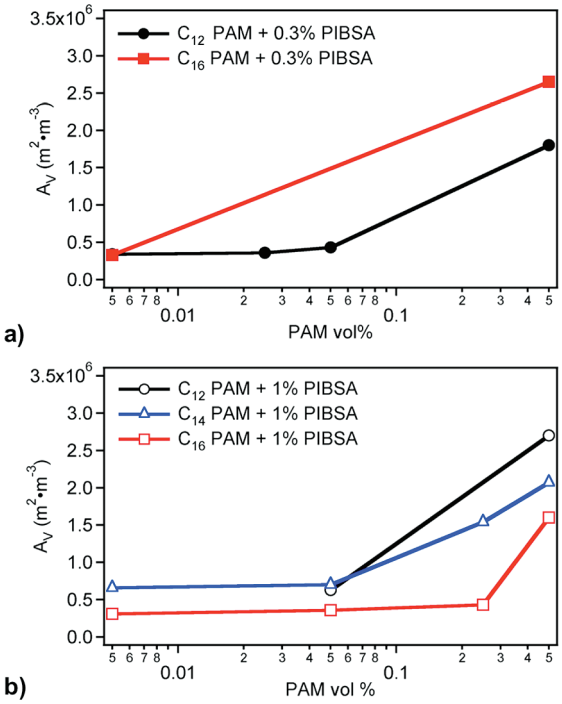

Figure 10. Interfacial surface area, A_V, at various C_{12}-PAM concentrations at 500 Hz for 0.3% (v/v) (a) and 1.0% (v/v) (b) PIBSA surfactant. The errors associated with the ordinate were not included but do not exceed $\pm 0.06\ m^2 \cdot m^{-3}$.

DISCUSSION

PIBSA-PAM Competition for the Aqueous/Oil Interface. Addition of PAM to the PIBSA-only emulsion causes a dramatic collapse in the observed emulsion yield stress. The small-angle scattering data show that this is connected with a collapse in the aqueous droplet/oil interfacial tension, due to some substitution of PIBSA by PAM at the interface. The first consequences of this appear as increased droplet elongation under stress, increased droplet polygonization, and increased emulsion refinement, but affecting viscosity to a much lesser extent. Additionally, the scattering data show that PAM can reach the micelles in the oil phase changing their structure.

The most obvious indication of the displacement of PIBSA from the aqueous interface by PAM coming from the water phase is the change in the micelle volume fraction as a function of PAM concentration in the emulsion preparation (Figure 6). The effect is fairly slight for the C_{12} PAM but strong for both the C_{14} and C_{16} PAMs that have greater hydrophobicity. The effect is also more noticeable for the emulsion made with 0.3% PIBSA where a change in micelle volume fraction of about a factor of 7 occurs. Since these data are measured for the CM systems that show the oil phase micelle content, the increase is unambiguously interpreted as displacement—especially since oil solubility of the PAM surfactants has been shown to be negligible.

Droplet/Oil Interfacial Tension. The most obvious difference observed between PAM and PIBSA-only containing emulsions was in yield stress. On inversion of a sample vial containing emulsion, PAM containing emulsions flow readily under gravity, while PIBSA-only emulsions do not. In emulsions that were allowed to rest for several days, the yield stress was distinctly larger indicating a shear history affect due to network formation even though the surface areas of these emulsions were similar to values obtained from other emulsions.

The experimental yield stress, τ_c, of a HIPE has been previously modeled by Princen[17] as:

$$\tau_c = A_v \sigma_{int} / 3\phi^{1/3} Y(\phi) \qquad (2)$$

σ_{int} is the interfacial tension, A_v is the interfacial area, and ϕ is the droplet volume fraction. $Y(\phi)$ is a dimensionless contribution to the yield stress and has been empirically fitted as: $Y(\phi) = 0.08 - 0.114 \log(1 - \phi)$.

Since the specific surface area values of PIBSA-only and low-PAM emulsions are roughly the same, as are the volume fractions, ϕ, the collapse in the yield stress on adding PAM is due to a collapse in σ_{int}. Using the observed interfacial surface area (Figure 10) and yield stress (Supporting Information, Table 3) we can obtain information regarding the interfacial tension. Typical examples are the 1% PIBSA emulsions. With no PAM σ_{int} is 8.3 $mN \cdot m^{-1}$. The addition of 0.05% C_{12}-PAM lowers this to 0.99 $mN \cdot m^{-1}$. Further addition of PAM to 0.5% content gives 0.17 $mN \cdot m^{-1}$ for C_{12}-PAM and 0.029 $mN \cdot m^{-1}$ for C_{16}-PAM. All of the emulsions tell a similar story; a small amount of PAM causes an interfacial tension collapse of about a factor of 10. Significant quantities of PAM further lower this. The effect is larger for the less hydrophilic C_{16}-PAM than for C_{12}-PAM. It seems that the PAM displaces PIBSA from the droplet/oil interface, with the more hydrophobic, although still water-soluble, C_{16}-PAM being, as expected, more effective in this displacement. We can calculate possible molecular coverage of the oil/aqueous interface from the amounts of PAM and PIBSA added, droplet surface areas, and assumed molecular conformations. At the very lowest PAM concentrations (0.005%) only part of the PIBSA can have been displaced. Nevertheless this partial displacement is enough to render the interface, and the surfactant monolayer attached there much less rigid.

The increases in specific surface area, A_V, shown in Figure 10 as a function of PAM volume percent in the emulsion are large. For the 0.5% PAM system a typical increase is of the order of 2 in surface area at 500 Hz. We note that for the PIBSA-only emulsion at this shear rate the surface area increase was about 3.5×10^4 $m^2 \cdot m^{-3}$ and 6×10^4 $m^2 \cdot m^{-3}$ for the 0.3% and 1% PIBSA systems, respectively (units: m^2 of surface per m^3 of emulsion). A further factor of 2 on this suggests considerable distortion of the spherical droplets by the shear field when PAM is present.

Shear Induced Droplet Elongation. Shear induces droplet elongation along the shear flow direction, resulting in the observed anisotropy in the SANS signal for both PIBSA-only and PIBSA/PAM emulsions. This anisotropy in the scattering from the contrast unmatched emulsions increases with the concentration of the PAM cosurfactant present (Figure 9). This anisotropy is insensitive to the cosurfactant tail chain length but reached values of up to 45% indicating a higher propensity for the PIBSA/PAM emulsions to elongate under shear than observed previously in PIBSA-only emulsions where the anisotropy was restricted to about 10%.

These higher deformations than shown by PIBSA-only emulsions are attributed to the significant reduction in interfacial tension at the oil/aqueous interface. An additional factor may be differential migration, on a scale of micrometers, of surfactant/cosurfactant at the interface.

Polygonization of Droplets. The extent of polygonization was modeled by "frac" as an isotropic effect in the fitting of the

circularly averaged SANS data. "Frac" may be expressed as the fraction of the average droplet surface engaged in contact with neighboring droplets, forming a bilayer. Typical values at a shear rate of 1 Hz for emulsions containing 0.3% PIBSA are 0.25 for PIBSA only, 0.27 with 0.5% C_{12}-PAM added, and 0.5 with C_{16}-PAM added. When sheared at 500 Hz these values decrease to 0.1, 0.2, and 0.4, respectively. The increase in frac at 1 Hz follows the trend in interfacial tension. The lower the interfacial tension, the higher the polygonal deformation. The reduction in deformation at 500 Hz is greatest for the most elastic interface (PIBSA only) and least for the most easily deformed. Thus the trends in droplet polygonization also follow directly from the interfacial tension.

Emulsion Refinement. The addition of PAM causes the droplet size of the emulsion to refine downward much faster during emulsion formation than with the PIBSA-only emulsions. Figure 10 shows that the higher the PAM concentration the higher is the specific surface area—and so the lower the mean droplet size—when sheared at 500 Hz. At higher shear rates further refinement of those emulsions with added PAM is less marked than with the PIBSA-only emulsions. The surface area of the PAM emulsions changes very little above shear rates of 500 Hz, unlike PIBSA-only emulsions. The refinement proceeds faster and easier in those emulsions in which the droplet/oil interfacial tension resists droplet elongation and division least.

Emulsion Viscosity. The viscosity of the PIBSA/PAM emulsions under shear behaves in very similar ways to that of the PIBSA-only emulsions—both shear thinning and thickening occur with similar viscosity values. Table 2 (Supporting Information) illustrates this similarity. An example is a 1% PIBSA emulsion at 1 Hz has a viscosity of 23.5 Pa·s, on adding 0.5% C_{12}-PAM this decreases, but only to 21.6 Pa·s. At 2000 Hz shear thinning has occurred, and the corresponding figures are 0.64 Pa·s and 0.54 Pa·s.

As in ref 1, shear thinning again occurs with negligible change in mean droplet size and change in surface area. The most likely mechanism for shear thinning is mainly the reduction of frac proportion of the interface (Figures 7 and 8): the proportion of a droplet's aqueous/oil interface to form a planar oil/aqueous/oil bilayer. As with PIBSA-only emulsions, an increase in the shear rate causes a decrease in the amount of bilayer, unsticking of droplet−droplet connections. As explained in more detail previously,[1] this "deflocculation" or structural breakdown results in shear thinning. Such a network breakdown is analogous to that described by Cross[18] and Mason and Bibette[19] leading to the formation of hydrodynamic clusters, "hydroclusters", as described by Melrose and Ball[20] and Wagner and Kalman.[21] Another source of shear thinning is the distortion of the droplet from spherical, as revealed by the increase in anisotropy (Figure 9), but this is probably less important. More theoretical work is required to confirm this speculation.

The shear thickening observed in successive 1 Hz "resting" periods stems from "refining" of the emulsion to smaller droplets at high shear rates already described above. SANS shows this clearly as an increase in the interfacial surface area. This results in higher emulsion viscosity. This droplet size effect also shows up macroscopically in the increased viscosity of the 1% PIBSA emulsions compared to the 0.3%. The addition of PAM has only small effects on viscosity at higher shear rates and displays no significant dependence on PAM tail chain length. There is a weak dependence of the viscosity on PAM concentration, with higher PAM concentrations lowering viscosities upon shearing. This again is due to PAM drastically lowering the droplet/oil interfacial surface tension and thus rendering the droplet more deformable under shear. The weak PAM dependence of the viscosity of these emulsions under shear shows a surprising relative independence to droplet rigidity. The viscosity seems to depend more strongly on droplet size. Since the droplet rigidity decreases markedly on addition of PAM, the inference is that under shear the droplets slide past one another without much transient local droplet deformation. If there were such distortion then we would expect the changed droplet rigidity to greatly lower viscosity in the PAM emulsions.

Surfactant Mobility at the Aqueous/Oil Interface. When contrast matched (CM) PIBSA-only and C_{12}-PAM CM emulsions are sheared, there is no noticeable anisotropy observed at the lowest Q values. We have previously interpreted this as due to immobility of the PIBSA surfactant at the oil−water interface.[1] If the surfactant maintained a constant footprint over all the distorted droplet, then the CM splitting would exactly mirror the UM. Even though the UM data indicate that the droplets deform, the only PIBSA "migration" is from the surfactant reservoirs in the oil (micelles + n-mers) to the very slightly increased droplet surface, a negligible effect. However the droplet deformation does increases the area of droplet "waist" and decreases area at the droplet "ends". This leads to more dense packing of immobile PIBSA surfactant on the droplet ends and more loosely around the waist of the droplet. The result is no anisotropy in these CM data. As Figure 9 parts b and d show, however, the C_{14}-PAM (triangles) and C_{16}-PAM (circles) data do show anisotropy in the CM data. This increases with PAM concentration, but there is no obvious trend between C_{14} and C_{16}. We also notice that the CM anisotropic splitting of the small-angle scattering intensity, while significant, is distinctly proportionately less than for the UM systems. This indicates that the higher molecular weight PAMs have been incorporated into the monolayer of PIBSA at the droplet surface, especially at higher PAM concentrations. The monolayer becomes much more mobile as a result and surfactant/cosurfactant can redistribute over micrometer scale distances to create a more uniform packing density at the surface. However the lesser splitting of CM compared to UM samples under shear shows that this response is not complete to reach uniform local surfactant density at the interface yielding uneven distributions of surfactant on the droplet. If there were no surfactant movement over the droplet surface then there would be no CM splitting. If the surfactant moved so as to maintain a constant footprint the UM and CM splitting would be the same. We observe an intermediate situation. The unequal distribution in surfactant under shear may also be the initial causes of droplet instability leading ultimately to droplet breakup.

Micellar Changes. Added PAM causes change in both micellar radii and the volume fraction of the micelles in the continuous oil phase (Supporting Information and Figure 6). At low PAM concentrations the average micellar radius shrinks from the 31(1) Å of the PIBSA-only emulsions down to 20(1) Å and is relatively independent of shear, as is the PIBSA-only value. The radius values increase as the PAM concentration increases. The effect is least for C_{12}-PAM and greater for C_{14}-PAM and C_{16}-PAM. The effect is also greater for the high PIBSA emulsions. We conclude that the PAM is able to reach the hydrophilic parts of the interior of the micelle—the core—but disrupts it, reducing the micelle stability and thus micellar size. The more hydrophobic C_{16}-PAM is more effective than the less hydrophobic C_{12}-PAM,

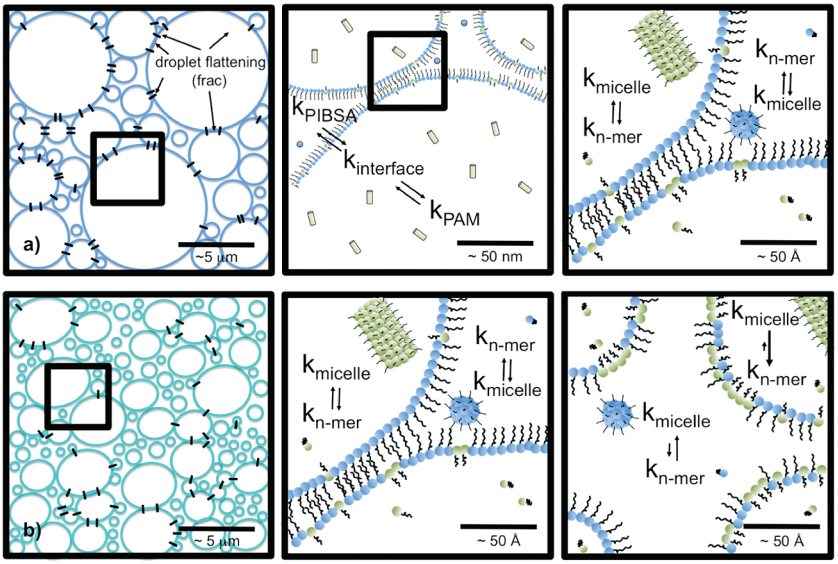

Figure 11. Illustration of the emulsion at various length scales in its quiescent state (a) and under an applied shear stress surpassing the τ_c (b). The change in color in the first panel of (b) from (a) is to reflect the higher concentration of PAM at the droplet interface. The black lines in most panels linking droplets indicate regions where droplet flattening occurs. The captions in the figures refer to the rates of surfactant migration in its various states and locations as a function of shear. Scale bars are only approximate. Above τ_c droplet distortion and refinement (b, leftmost panel) with redistribution of the PIBSA and PAM surfactants obtained by a two-stage process from surfactant micelles present in the oil and water phases (b, panels 2 and 3 from the left). Droplet distortion and refinement causes a reduction in the amount of droplet flattening as indicated by the frac parameter.

perhaps because the tail size matches the PIBSA better. The mechanism of the strongly oil insoluble PAM reaching the oil soluble micelles is not clear, but probably related to the equally mysterious mechanism of water being present in the micelles.

As PAM concentrations increase the micelles swell for C_{14}-PAM and C_{16}-PAM, but not much for C_{12}-PAM. We attribute this swelling to the micelle attracting increased aqueous/acrylic content in the core, which expands greatly. This is of course a restatement of the "wedge" theory of micelle size in slightly different terms. The micelle becomes more hydrophilic. This agrees with our observation that in PIBSA-only emulsions those with lower molecular weight, more hydrophilic, PIBSA contain larger micelles with higher water content in the core than those containing higher molecular weight, more hydrophobic, PIBSA.[4,5] This conclusion is supported by values of the micelle volume fractions. We would expect an increase in core content to increase the volume fraction above that for PIBSA-only values. Again we observe higher volume fractions for C_{14}-PAM and C_{16}-PAM than we see for C_{12}-PAM or PIBSA-only emulsions. This again is indirect evidence of micellar swelling due to incorporation of more water/acrylic in the micelle core.

Model fitting was conducted separately on both the horizontal and vertical portions of the integrated intensities for the contrast matched data. Results show a consistent slight significant difference of 1−2 Å in values of the micelle radius between horizontal and vertical data with larger values found in the horizontal data indicating possible slight elongation of the micelles is occurring along the applied shear field. This is a small difference, but its consistent presence in the fitted results and a consideration of propagated errors leads us to believe in its reality. Using the same refining procedure this effect was not present in any experiments performed on PIBSA emulsions under shear. This again indicates that there is PAM cosurfactant present in the reverse micelles in the oil phase, making the micelle less stable and slightly deformable under shear.

The values of $\phi_{micelle}$ show a similar decrease in values under shear as did the PIBSA-only systems, but with less recovery in population when a low shear is subsequently applied. The lack of recovery could indicate that displaced PIBSA is not participating as effectively as the PAM cosurfactant in coating newly formed interfaces when sheared. This alters the distribution of surfactant and cosurfactant at the oil/aqueous interface leaving more PIBSA dissolved in the oil phase as micelles, which is reflected in Figure 6.

CONCLUSIONS

Using a combination of SANS and in situ rheological measurements, we are able to relate the macroscopic physical behavior of PIBSA-stabilized aqueous-in-oil HIPEs with varying concentrations and types of PAM cosurfactants under shear to their nano- and microscopic structure and dynamics. The addition of cosurfactant, even in very small quantities, lowers the oil/aqueous interfacial tension by a factor of 10−100, making the interface much less rigid. The effect increases when we increase the PAM's hydrophobic tail length from C_{12} to C_{16}. An explanation for both effects is that PAM is displacing some, or at higher PAM concentrations all, of the PIBSA from the aqueous droplet/oil interface. On addition of PAM there are large decreases in yield stress and increased droplet polygonization (droplet−droplet touching) when at rest. When the emulsion is sheared the droplets deform along the shear direction much more, and droplet−droplet touching is less disrupted than in PIBSA-only emulsions. Lastly, emulsion refinement—droplet size reduction—is somewhat enhanced by addition of PAM. These are all consequences of the collapse in interfacial tension. However this much larger droplet deformability does NOT appreciably lower the viscosity. The addition of the aqueous-soluble PAM cosurfactant does not alter the emulsions' viscosity markedly. The shear thinning due to disruption of networks of

touching droplets still occurs, as does the shear thickening due to emulsion refinement, but changes in both are much smaller than in properties more dependent on droplet rigidity. Droplet sizes and droplet−droplet touching regimes dominate the viscous behavior, and droplet rigidity is less important. We infer from this that droplet motion under shear does not involve much transient droplet deformation as the droplets move by each other. Emulsion refinement is closely related to this. Critical capillary numbers, Ca_{crit}, defined as $<\eta(D)DR_{32}>/\sigma_{int}$,[22] where $\eta(D)$ is the viscosity at a shear rate D, for concentrated emulsions do accurately model shear stresses at which droplet breakup occurs in our emulsions. This result is similar to what we found in the PIBSA-only emulsions. But our results for the values of Ca_{crit} are much lower than previous empirical results by Grace.[23] This is most likely also, as for viscosity, due to the lack of accounting for droplet−droplet multibody interactions, complicated by high polydispersity creating Apollonian-like sphere packing, in these high-internal volume fraction emulsions.

A further observation concerns the enhanced mobility of PAM compared to PIBSA at the aqueous droplet/oil interface. On droplet deformation the stabilizing monolayer, with PAM in it, is able to relax to equilibrium over a micrometer scale, which the PIBSA-only emulsions cannot. The PAM, although oil insoluble, is also capable of migrating into the nanoscale micelles of PIBSA distributed in the continuous oil phase, changing the micellar properties in ways predictable from hydrophilic/hydrophobic properties of the PIBSA and PAM molecules. Figure 11 summarizes our observations and conclusions from our rheo-SANS results. This illustrates what we think is occurring in the PIBSA/PAM emulsion under the influence of an applied shear.

We have shown in these emulsions that, if we use both an oil soluble surfactant and very small quantities of a water-soluble surfactant, we gain sufficient freedom to manipulate properties dependent on the oil/water interface and those on the bulk oil/continuous phases. This uncoupling may be useful in emulsion design.

■ ASSOCIATED CONTENT

Ⓢ Supporting Information. Details of the block copolymer (PAM) synthesis, the amounts of each constituent in the emulsions (Table 1), details of emulsion rheology (Table 2, shear stress as a function of applied shear for all emulsions), Table 3 (yield stress values, in units of Pa, obtained from y-intercept values extrapolated from shear stress versus shear rate plots), Table 4 [yield stress (in Pa) values obtained from Princen (equation 2)[17]], and model fitting of isotropically averaged SANS data. Model fit parameters of the SANS data from all contrast matched (CM) and contrast unmatched (UM) emulsions as a function of the shear profile applied in Figure 2; Tables 5 and 6, anisotropic SANS data; Table 7, SANS anisotropy (%) at 500 Hz shear interval. This material is available free of charge via the Internet at http://pubs.acs.org.

■ AUTHOR INFORMATION

Corresponding Author

*E-mail: jww@rsc.anu.edu.au. Fax: 02 6125 0750. Tel.: 02 6125 3575.

■ ACKNOWLEDGMENT

We thank the Rutherford Appleton Laboratory for access to the LOQ instrument at ISIS and Dr. Ann Terry and Dr. Stephen Holt for their assistance. Travel grants, through the Australian Government ISTAC/ANSTO Access to Major Facilities Program and the AINSE/ARC international access to ISIS, are gratefully acknowledged. This work was partly financed by the Australian Research Council with SPIRT and SRF awards joint with Orica Ltd.

■ REFERENCES

(1) Yaron, P. N.; Reynolds, P. A.; Mata, J. P.; McGillivray, D. J.; White, J. W. *J. Phys. Chem. B* **2010**, *114*, 3500–3509.
(2) Reynolds, P. A.; Gilbert, E. P.; White, J. W. *J. Phys. Chem. B* **2000**, *104*, 7012–7022.
(3) Reynolds, P. A.; Gilbert, E. P.; White, J. W. *J. Phys. Chem. B* **2001**, *105*, 6925–6932.
(4) Reynolds, P. A.; Gilbert, E. P.; Henderson, M. J.; McGillivray, D. J.; White, J. W. *J. Phys. Chem. B* **2009**, *113*, 12231–12242.
(5) Reynolds, P. A.; Gilbert, E. P.; Henderson, M. J.; McGillivray, D. J.; White, J. W. *J. Phys. Chem. B* **2009**, *113*, 12243–12256.
(6) Reynolds, P. A.; McGillivray, D. J.; Mata, J. P.; Yaron, P. N.; White, J. W. *J. Colloid Interface Sci.* **2010**, *349*, 544–553.
(7) Baranyai, K. J.; Reynolds, P. A.; Henderson; M. J.; White, J. W., in preparation.
(8) Reynolds, P. A.; Baranyai, K. J.; Jackson, A. J.; Henderson, M. J.; Zank, J.; Scott, A. J.; White, J. W., in preparation.
(9) Ferguson, C. J.; Hughes, R. J.; Pham, B. T. T.; Hawkett, B. S.; Gilbert, R. G.; Serelis, A. K.; Such, C. S. *Macromolecules* **2002**, *35* (25), 9243–9245.
(10) Scott, A. J.; Zank, J.; White, J. W., in preparation.
(11) Mata, J. P.; Narayanan, T.; White, J. W., in preparation.
(12) Heenan, R.; King, S. *ISIS User Guide*; Boland, B., Whapham, S., Eds.; ISIS, Rutherford Appleton Laboratory: Didcot, 1992.
(13) King, S. *Modern Techniques for Polymer Characterization*; Pethrick, R. A., Dawkins, J. V., Eds.; Wiley: New York, 1999; Ch. 7, p 171.
(14) Griffith, W. L.; Triolo, R.; Compere, A. L. *Phys. Rev. A* **1987**, *35* (5), 2200–2206.
(15) Kotlarchyk, M.; Chen, S.-H.; Huang, J. S. *J. Phys. Chem.* **1982**, *86* (17), 3273–3276.
(16) Pal, R. *Food Hydrocolloids* **2006**, *20*, 997–1005.
(17) Princen, H. M. *J. Colloid Interface Sci.* **1985**, *105*, 150–171.
(18) Cross, M. M. *J. Colloid Sci.* **1965**, *20*, 417–437.
(19) Mason, T. G.; Bibette, J. *Langmuir* **1997**, *13*, 4600–4613.
(20) Melrose, J. R.; Ball, R. C. *J. Rheol.* **2004**, *48* (5), 961–978.
(21) Kalman, D. P.; Wagner, N. J. *Rheol. Acta* **2009**, *48*, 897–908.
(22) Jansen, K. M. B.; Agterof, W. G. M.; Mellema, J. *J. Rheol.* **2001**, *45*, 227–236.
(23) Grace, H. P. *Chem. Eng. Commun.* **1982**, *14*, 225–277.